

AD-787 781

INTEGRATED OPTICS

G. Sanjiv Kamath, et al

Hughes Research Laboratories

Prepared for:

Air Force Cambridge Research Laboratories

January 1974

DISTRIBUTED BY:

**NTIS**

National Technical Information Service  
U. S. DEPARTMENT OF COMMERCE

AD 787781

AFCRL - TR - 74 - 0392

## INTEGRATED OPTICS

G. SANJIV KAMATH  
AMNON YARIV  
R. G. HUNSPERGER  
MICHAEL BARNOSKI  
KYOHEI SAKUDA  
VIKTOR EVTUHOV

HUGHES RESEARCH LABORATORIES  
3011 MALIBU CANYON ROAD  
MALIBU, CALIFORNIA 90265

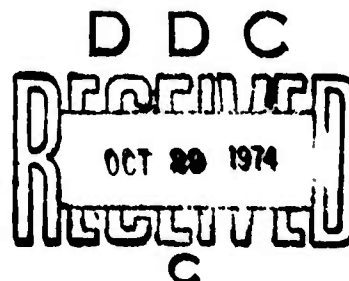
JANUARY 1974

SEMIANNUAL TECHNICAL REPORT 3  
CONTRACT F19628-72-C-0322

APPROVED FOR PUBLIC RELEASE; DISTRIBUTION UNLIMITED.

Sponsored by  
DEFENSE ADVANCED RESEARCH PROJECTS AGENCY  
ARPA ORDER 2074

Monitored by  
AIR FORCE CAMBRIDGE RESEARCH LABORATORIES  
AIR FORCE SYSTEMS COMMAND  
UNITED STATES AIR FORCE  
HANSCOM AFB, MASSACHUSETTS 01730



Reproduced by  
NATIONAL TECHNICAL  
INFORMATION SERVICE  
U S Department of Commerce  
Springfield VA 22151

ARPA Order No. 2074

Program Code No. 2D10

Contractor: Hughes Research Laboratories

Effective Date of Contract, 1 June 1972

Contract No. F19628-72-C-0322

Principal Investigator and Phone No.

G. Sanjiv Kamath, (213)456-6411, Ext. 210

Amnon Yariv, (213)795-6841

AFCRL Project Scientist and Phone No.

Dr. Freeman D. Shepherd, Jr. (617)861-2225

Contract Expiration Date: 30 August 1974

ACCT. NO. 12	
PTIS	White Section <input checked="" type="checkbox"/>
D. C.	Buff Section <input type="checkbox"/>
UNCLASSIFIED	<input type="checkbox"/>
JULY 1974	
BY	
DISTRIBUTION/AVAILABILITY CODES	
SPECIAL	
A	

Qualified requestors may obtain additional copies from the Defense Documentation Center. All others should apply to the National Technical Information Service.

UNCLASSIFIED

AD 787 781

SECURITY CLASSIFICATION OF THIS PAGE (When Data Entered)

REPORT DOCUMENTATION PAGE		READ INSTRUCTIONS BEFORE COMPLETING FORM
1. REPORT NUMBER AFCRL-TR-74-0392	2. GOVT ACCESSION NO.	3. RECIPIENT'S CATALOG NUMBER
4. TITLE (and Subtitle)  INTEGRATED OPTICS		5. TYPE OF REPORT & PERIOD COVERED Semiannual Tech. Report July 1973 - Dec. 1973
		6. PERFORMING ORG. REPORT NUMBER Semiannual Tech. Rpt. 3
7. AUTHOR(s) G. Sanjiv Kamath      Michael Barnoski Amnon Yariv          Kyohei Sakuda R.G. Hunsperger      Viktor Evtuhov		8. CONTRACT OR GRANT NUMBER(s) F19628-72-C-0322
9. PERFORMING ORGANIZATION NAME AND ADDRESS Hughes Research Laboratories 3011 Malibu Canyon Road Malibu, California 90265		10. PROGRAM ELEMENT, PROJECT, TASK AREA & WORK UNIT NUMBERS 61101D, 2074 T n/a WU r/a
11. CONTROLLING OFFICE NAME AND ADDRESS		12. REPORT DATE January 1974
		13. NUMBER OF PAGES 63
14. MONITORING AGENCY NAME & ADDRESS (if different from Controlling Office) Air Force Cambridge Research Laboratories (LQ) Hanscom AFB, Massachusetts 01730 Contract Monitor: F.D. Shepherd Jr./LQD		15. SECURITY CLASS (of this report)  Unclassified
16. DISTRIBUTION STATEMENT (of this Report)  A - Approved for public release; distribution unlimited.		
17. DISTRIBUTION STATEMENT (of the abstract entered in Block 20, if different from Report)		
18. SUPPLEMENTARY NOTES  This research was supported by the Defense Advanced Research Projects Agency. ARPA Order No. 2074.		
19. KEY WORDS (Continue on reverse side if necessary and identify by block number)  GaAs, Ga <sub>1-x</sub> Al <sub>x</sub> As, Epitaxy, Integrated Optics, Waveguides, Periodic Structures		
20. ABSTRACT (Continue on reverse side if necessary and identify by block number)  During this reporting period emphasis was placed mainly on improving growth techniques for epitaxial layers by the slide bar and the infinite melt methods. New slide bar assemblies made from pyrolytic graphite have eliminated many of the imperfections previously observed. More than a dozen layers were grown in the new system. 63		

DD FORM 1473 1 JAN 73 EDITION OF 1 NOV 65 IS OBSOLETE

Reproduced by  
NATIONAL TECHNICAL  
INFORMATION SERVICE  
U S Department of Commerce  
Springfield VA 22151

Unclassified

SECURITY CLASSIFICATION OF THIS PAGE (When Data Entered)

UNCLASSIFIED

SECURITY CLASSIFICATION OF THIS PAGE(When Data Entered)

with carrier concentrations  $\sim 10^{16}/\text{cm}^3$  and mobilities in excess of  $4000 \text{ cm}^2/\text{Vs}$ . Waveguiding of  $1.15\text{-}\mu\text{m}$  light has been observed in these layers, made possible by the graded aluminum concentration profile which results from the limited melt and the segregation effect. Multi-layer waveguide structures have also been grown using the limited melt method. About 75 layers grown in a series by the infinite melt method have been characterized by electron beam microprobing and Hall measurements. Surface variation of the aluminum concentration has been determined to be typically 5 to 6% or less. Mobilities  $\cong 4500 \text{ cm}^2/\text{Vs}$  have been measured in samples with carrier concentrations  $\cong 2 \times 10^{15}/\text{cm}^3$ . As part of the continuing effort to evaluate device elements for which GaAs and (GaAl)As are particularly suitable, we have performed an analysis of an integral waveguide/detector in which proton bombardment was used to produce sensitivity to wavelengths  $> 0.9 \mu\text{m}$ . Calculations of projected performance indicate that quantum efficiency of at least 60% should be obtainable for  $\lambda \cong 1 \mu\text{m}$ . We have also evaluated the projected performance of "leaky" waveguides for which the guide index is less than that of the substrate. The results of this analysis show that useful integrated optical devices for  $0.8 \mu\text{m}$  light can be fabricated using leaky waveguides, provided the guide height is  $\geq 10 \mu\text{m}$ . In this case the loss due to leakage is  $< 1 \text{ cm}^{-1}$  for an aluminum concentration  $> 20\%$ .

UNCLASSIFIED

SECURITY CLASSIFICATION OF THIS PAGE(When Data Entered)

## TABLE OF CONTENTS

I.	INTRODUCTION AND SUMMARY . . . . .	7
	A. GaAs and Ga <sub>1-x</sub> Al <sub>x</sub> As Epitaxial Layer Growth . . . . .	8
	B. Materials Evaluation . . . . .	8
	C. Device Elements. . . . .	9
II.	LIMITED MELT LIQUID EPITAXY. . . . .	11
	A. Materials Growth . . . . .	11
	B. Epitaxial Layer Characterization . . . . .	12
III.	INFINITE MELT LIQUID EPITAXY . . . . .	23
	A. Materials Growth . . . . .	23
	B. Epitaxial Layer Characterization . . . . .	24
IV.	DEVICE ELEMENTS. . . . .	31
	A. Analysis of Proton Implanted Integrated Waveguide/Detector. . . . .	31
	B. Analysis of "Leaky" Waveguides . . . . .	37
V.	FUTURE PLANS . . . . .	43
	REFERENCES . . . . .	45
	APPENDIX . . . . .	47

## LIST OF ILLUSTRATIONS

Fig. 1.	Limited melt liquid epi sample No. 122 . . . . .	13
Fig. 2.	Electron microprobe profile of epitaxial layer surface — (limited melt slide bar) . . . . .	16
Fig. 3.	Aluminum concentration profile in limited melt epitaxial layer on a 10° bevel in cross section . . . . .	17
Fig. 4.	Waveguided light in a (GaAl)As layer with graded aluminum concen- tration . . . . .	19
Fig. 5.	A double layer of $Ga_{1-y}Al_yAs/Ga_{1-x}Al_xAs$ grown on GaAs . . . . .	20
Fig. 6.	Aluminum concentration profile on $\infty$ melt LEPI layers (surface of epilayer) . . . . .	27
Fig. 7.	Aluminum concentration profile in $\infty$ melt liquid epitaxial layers on a 30° bevel in cross section . . . . .	28
Fig. 8.	Proton-implanted integrated optical detector — device geometry. . . . .	32
Fig. 9.	Principle of operation of integrated detector. . . . .	34
Fig. 10.	Dielectric waveguide configuration. . . . .	37

**Preceding page blank**

## I. INTRODUCTION AND SUMMARY

The objectives of this contract are to study and analyze the propagation, attenuation, modulation, and detection of coherent optical waves in thin film waveguides, in particular epitaxial semiconductor structures at a wavelength of  $8500 \text{ \AA}$ , to determine the parameters controlling the solution regrowth epitaxy of the  $\text{Ga}_{1-x}\text{Al}_x\text{As}$  system, to study the influence of the index discontinuity and semiconductor carrier concentration on optical properties, and to develop the elementary optical device elements.

This report covers the work performed during the period of July 1973 through December 1973. The present program may be viewed as consisting of the following elements: (1) Establishment of epilayer material and structural requirements, (2) Development of materials growth techniques, (3) materials evaluation, and (4) device analysis and fabrication techniques. The epilayer material and structural requirements from the device point of view have been tentatively established as described in Semiannual Report No. 2 (August 1973). Hence, no work was done on that phase of the program during this reporting period. That phase will, of course, be reactivated if and when experimental data from waveguides or devices indicate that a reevaluation of requirements is needed. The materials growth techniques presently being developed involve slide-bar (limited melt) and vertical dipping (infinite melt) liquid phase epitaxy. Vapor phase epitaxy has been evaluated as described in Semiannual Report No. 2. Materials evaluation includes microprobe, photoluminescence and x-ray analysis, Hall effect and C-V measurements, and determination of waveguiding properties and losses of the films. The last element of the program is directed toward establishing specific materials requirements for integrated optics devices and development of fabrication techniques for rudimentary devices. For this task some of the company-supported efforts in specific device areas are especially helpful. In particular, a company-funded program to develop an integrated waveguide/photodetector has produced encouraging preliminary

Preceding page blank



results in GaAs, and we feel the fabrication methods used can be applied advantageously to (GaAl)As optical integrated circuits.

A. GaAs and  $\text{Ga}_{1-x}\text{Al}_x\text{As}$  Epitaxial Layer Growth

During this period emphasis was mainly on improving growth techniques for epitaxial layers by the slide bar and the infinite melt method. The layers grown by the slide bar method showed imperfections in the interfaces between layers. New slide bar assemblies made from pyrolytic graphite have eliminated many of these. In addition, processing conditions have been optimized to permit scratch-free wiping of the melt at the end of each layer growth. More than a dozen layers were grown in the improved system. These layers are being characterized and their waveguiding properties determined. The quality of the layers is very good, with carrier concentrations  $\sim 10^{16}/\text{cm}^3$  and mobilities in excess of  $4000 \text{ cm}^2/\text{Vsec}$ . Waveguiding of  $1.15 \mu\text{m}$  light has been demonstrated in some of these layers. The infinite melt growth of (GaAl)As has been perfected and a series of layers with varying aluminum concentration have been grown from one melt.

B. Materials Evaluation

About 75 layers grown in a series by the infinite melt method have been characterized and the stability of the melt during long residence in the growth chamber established. The Al concentration profiles have been established by electron beam microprobing of cleaved cross sections, and Hall measurements have been used to determine carrier concentrations and mobilities. Surface variation of the aluminum concentrations is typically 5 to 6% or less. Mobilities  $\approx 4500 \text{ cm}^2/\text{Vsec}$  have been measured in samples with carrier concentrations  $\approx 2 \times 10^{15}/\text{cm}^3$ . Preliminary optical waveguiding evaluations have been performed on some of these samples. Large area layers obtained by this method will now be used as the basic building block for integrated

optics. The optical absorption of the alloy as a function of aluminum concentration is being investigated using these layers.

### C. Device Elements

We have considered device elements for which GaAs and (GaAl)As are particularly suitable with the aim of establishing the relationship between device requirements and material and structure characteristics. Components such as waveguide bends and couplers, distributed feedback injection lasers, integrated detectors, modulators, and periodic optical filters have been considered, as described in Semiannual Report No. 2. During this reporting period we have paid particular attention to the integrated detector. A company funded program to develop a method for forming integrated waveguide/detectors in GaAs has produced encouraging preliminary results. Proton bombardment has been used to create the required absorbing centers in the detector volume. Detectors have been fabricated with a quantum efficiency of 17% and a pulse response time less than 200 nsec, and it is felt that further development of the technique will yield devices with significantly improved characteristics. We have performed an analysis of the proton implanted detector which indicates that the same basic fabrication methods used in GaAs should be applicable to (GaAl)As. Projections based on the GaAs data indicate that a (GaAl)As waveguide/detector operating at  $\lambda = 9000 \text{ \AA}$  with a GaAs LED or laser source is feasible.

## II. LIMITED MELT LIQUID EPITAXY

### A. Materials Growth

During the last six months the primary emphasis in materials growth was on developing smooth uniform epitaxial layers of (GaAl)As for use in waveguides. The limited melt (graphite slide bar) and the infinite melt techniques were both improved to grow the layers. The new pyrolytic graphite slide bar was used and the processing conditions for layer growth determined. More than a dozen layers were grown using it and the layer characteristics determined by electron microprobe and Hall measurements. These layers have proved to have interesting applications as waveguides and their optical characteristics are being determined.

The system used and the theory behind the technique have been given in our previous reports. Several significant improvements have been made in our growth system.

1. A transfer chamber has been added at the tail end of the growth chamber.
2. The gas flow has been altered to minimize contamination.
3. A new graphite assembly made of pyrolytic graphite, incorporating alterations in mechanical design, has been used successfully to improve the surface quality of the layers. These steps have resulted in improved reproducibility of the layers and also lower impurity levels and smoother surfaces. Details are given below.

The transfer chamber, which is an extension of the quartz growth tube outside the furnace, allows us to move the slide bar assembly into, and out of, the furnace without exposing the graphite to air. The slide bar with the melt, the source and the substrate are placed in the transfer chamber, and the whole tube flushed with hydrogen until all traces of air are removed before the slide bar is pushed into the growth chamber. This has eliminated occasional evidence of oxidation of the melt surface causing bad wiping action and some scratching of the surface of the grown layer. When the slide bar is removed after

growth, it is allowed to cool to room temperature in hydrogen before being extracted. This procedure has minimized the tailing of gallium over the graphite making it difficult to reuse the slide bar without elaborate cleaning between successive runs. Such cleaning should be kept to a minimum in practice, to minimize the risk of contamination. The transfer chamber has helped considerably, and the use of pyrolytic graphite has further alleviated the problem.

Another significant improvement in the present system results from optimizing the gas flow pattern in the growth chamber. Provision has now been made to introduce both hydrogen and nitrogen into the input side of the tube without interference with each other. The tube is evacuated from the extension transfer chamber so that no gas is ever allowed to flow from the tail end to the front. Provision has also been made to supply an independent input of nitrogen to the transfer tube so that it could be filled and evacuated without having to disturb the flow through the main growth chamber.

Apart from using pyrolytic graphite as the slide bar material, the geometry of the melt wells has been altered to minimize the travel of the slide bar during the wiping operation. The construction also enables better registration of the melt cavity with the substrate position, permitting more uniform growth over the whole substrate, and eliminating problems due to uneven growth at the edges of the substrate. The results are shown in the smooth layers shown in Fig. 1.

#### B. Epitaxial Layer Characterization

Over a dozen layers have been grown using the pyrolytic graphite slide bar assembly. The characteristics of the layer are shown in Table I. The values of thickness of layers obtained is proof of the reproducibility of the process. Thickness control is an essential consideration in the fabrication of single mode waveguides, as explained in the previous report. The quality of the layer can be seen from the carrier concentration in the  $10^{16}/\text{cm}^3$ , and mobilities in excess of  $4000 \text{ cm}^2/\text{Vs}$  obtained for the epitaxial layers. Since the slide bar

2957-10

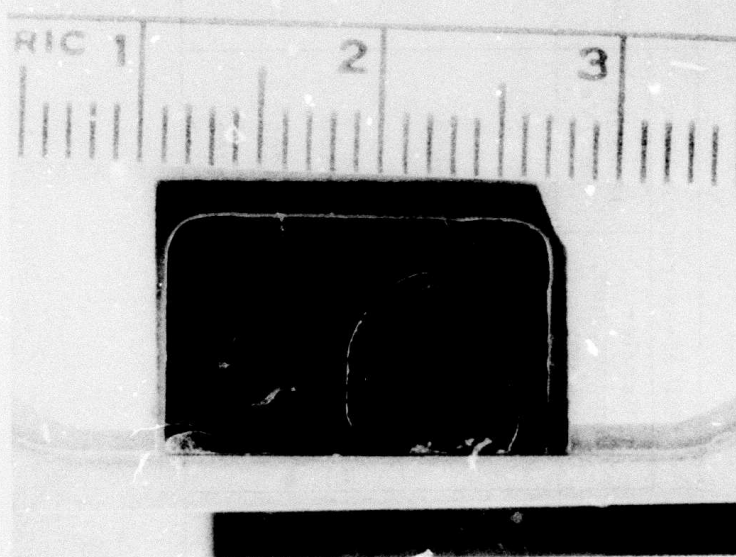


Fig. 1. Limited melt liquid epi sample No. 122. Note the smooth surface. The as-grown surface shows a slight amount of residual melt at the right; this problem can be minimized by reducing the gap between the grown layer and the graphite wiping surface.

TABLE I  
Ga<sub>1-x</sub>Al<sub>x</sub>As Epitaxial Layer (slide bar) Characteristics

Sample No.	Growth Temperature, °C	Thickness, $\mu\text{m}$	Hall Measurement Data		Aluminum Concentration, X
			Carrier Concentration, N/cm <sup>3</sup>	Mobility, cm <sup>2</sup> /Vs	
0112	886	2.9	$1.6 \times 10^{15}$	4600	0.2
0113	886	2.9			
0114	885	2.3			
0120	889	3.5	$1.08 \times 10^{16}$	4100	
0121	888	3.5		4200	
0122	888	4.5		4200	

T1193

method suffers from a large surface-to-volume ratio for the melt in the well, this has to be considered an exceptionally low level of impurity, and the mobility value is a strong indication of the low degree of compensation in the layer. It may be worth mentioning that when graphite containers are used, the first layers obtained show some compensation presumably due to surface impurities. After a series of runs are made with the same graphite piece, the layers stabilize to an "undoped" characteristic as shown in our present series.

Figures 2 and 3 give a representation of the electron microprobe profile of the layers for aluminum concentration. Figure 2 is a profile of the surface and gives an idea of the variation of aluminum concentration inherent to the growth process in our system. This should be compared to the layers made in our early experiment, using our old growth system and slide bar assembly. Whereas we see a variation of  $\sim \pm 6\%$  now, we used to see as much as  $\pm 15\%$  in the old results.

Figure 3 is a graphical representation of the aluminum concentration profile in the cross section of the beveled layer. Problems of accurate determination of the profile are complicated by the very thin layers involved. The measurement is made somewhat more convenient by using a beveled layer with  $1^\circ$  angle. The main difficulty is that the shallow angle makes the region, close to the junction, very thin and hence the electron beam penetration, even with low energy, goes beyond the epitaxial layer. Since the volume element seen by the electron beam encompasses an aluminum-free region, corrections have to be made to obtain the true concentration in the epitaxial layer only. The definition of the junction is also somewhat difficult by a simple examination of the x-ray scattering data.

To overcome this problem we decided to start from the surface of the layer at the other end of the bevel and work toward the junction, since the thickness of the layer is independently verifiable. In this procedure, the complication arises due to the processing steps involved. When the bevel is finished it has to be etched chemically to remove the mechanically damaged surface. The etch results in a rounding of the edges of the bevel, making it difficult to pinpoint the top surface of the

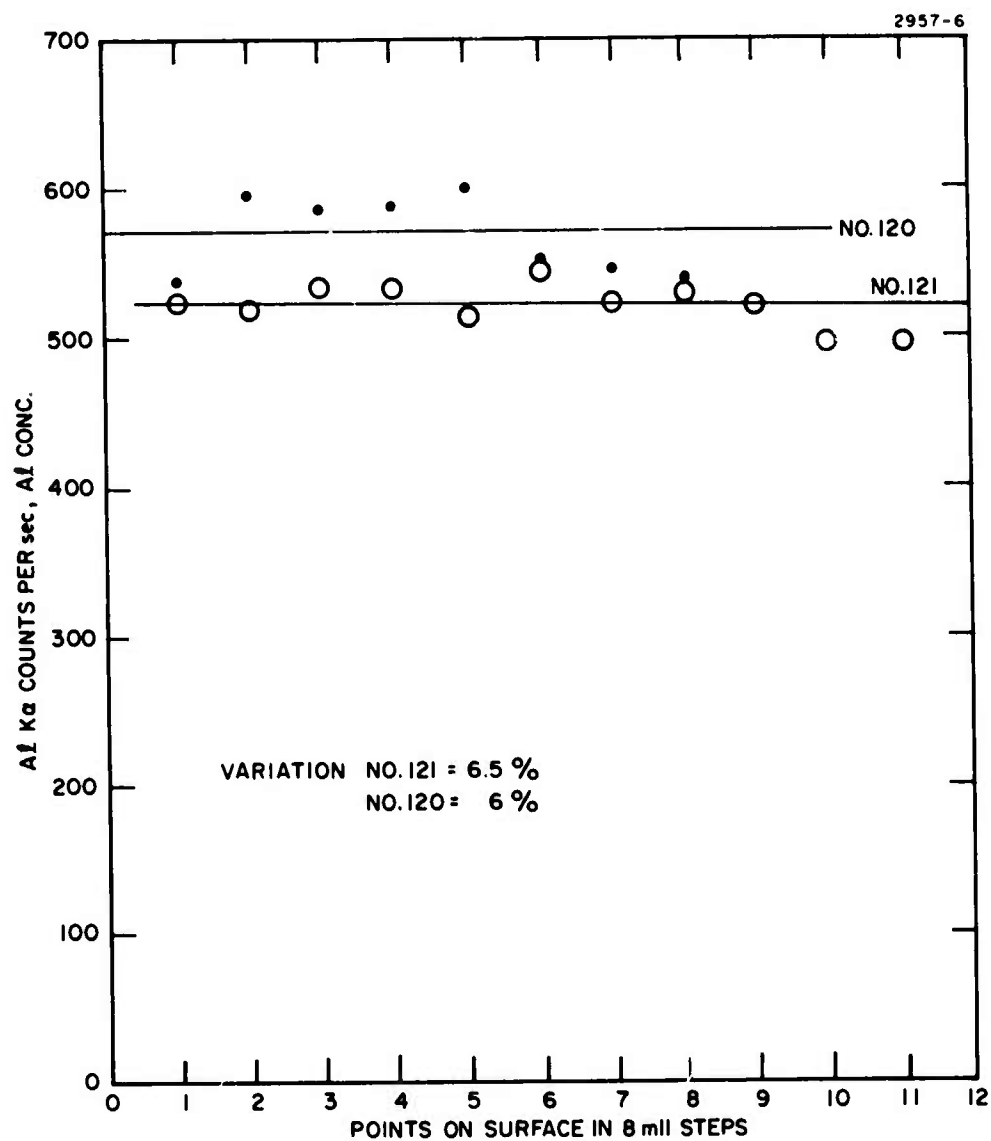


Fig. 2. Electron microprobe profile of epitaxial layer surface — limited melt slide bar).



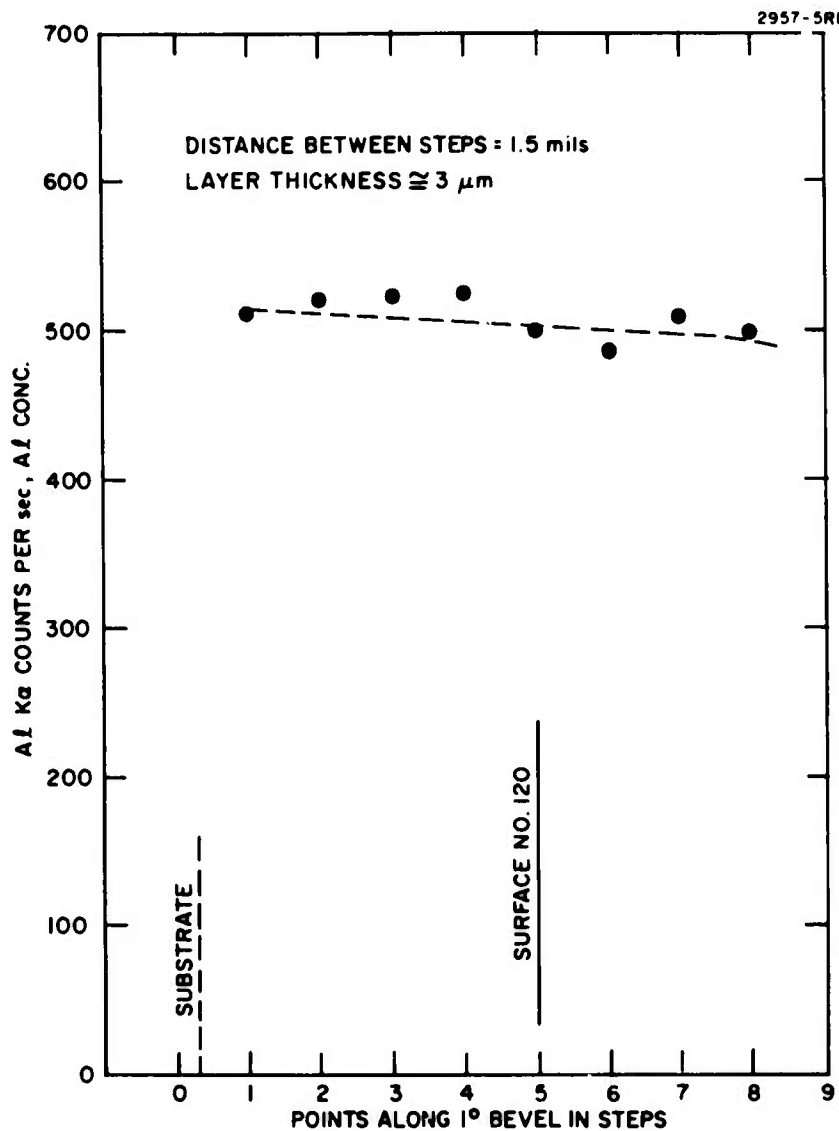


Fig. 3. Aluminum concentration profile in limited melt epitaxial layer on a 1° bevel in cross section.

epitaxial layer during microprobe analysis. We have resorted to depositing a thin layer of gold on the top surface before beveling to avoid this problem. By using different beveling angles and varying electron beam energies in a series of measurements, we are setting up a program that will enable us to make accurate measurements of the aluminum concentration profile in the region close to the growth junction. It can be seen from the results, however, that for thicknesses in the range of 2 to 3  $\mu\text{m}$ , the slide bar method can produce layers which do not have too severe a gradient in aluminum concentration. A more quantitative evaluation of the gradient in thin layers will have to await some refinement in measurement techniques presently being developed.

Such measurements are of special significance since we have been able to demonstrate that the epitaxial layer of (GaAl)As grown on GaAs can be used as a waveguide. The result is to be expected if, at the junction, aluminum concentration is highest and then drops off towards the surface; the decreasing aluminum concentration will be reflected in an increasing refractive index in the layer from the junction to the surface. Figure 4 shows the transverse intensity distribution of 1.15  $\mu\text{m}$  light being transmitted through such a guide. Since the graded layer is easy to grow, because of the high segregation coefficient of aluminum during growth from solution, it would be highly instructive to study waveguiding characteristics as a function of the aluminum profile. We hope to study this problem in detail, using both the slide bar epitaxy as well as the infinite melt epitaxy.

About a dozen layers of (GaAl)As have been grown using the new pyrolytic graphite assembly and the improved growth chamber mentioned in the previous paragraphs. These experiments have helped define the growth parameters and processing procedures necessary to optimize layer growth at  $\sim 800^\circ\text{C}$ . Using these as a guide, a few double layers of (GaAl)As also have been grown. These are now being analyzed using the electron microprobe and being investigated as waveguides. An example of such a layer is shown in Fig. 5. The main improvement over the layers described in our previous report is in two aspects. (1) We have now enough growth data to make reproducible

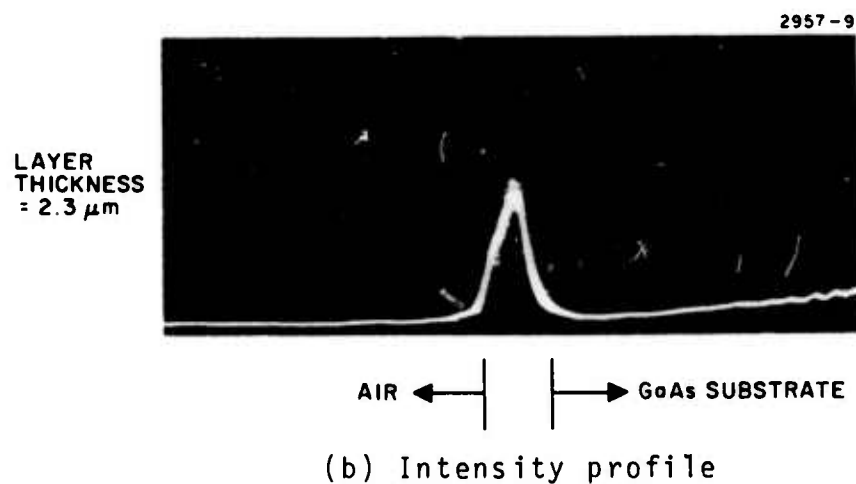
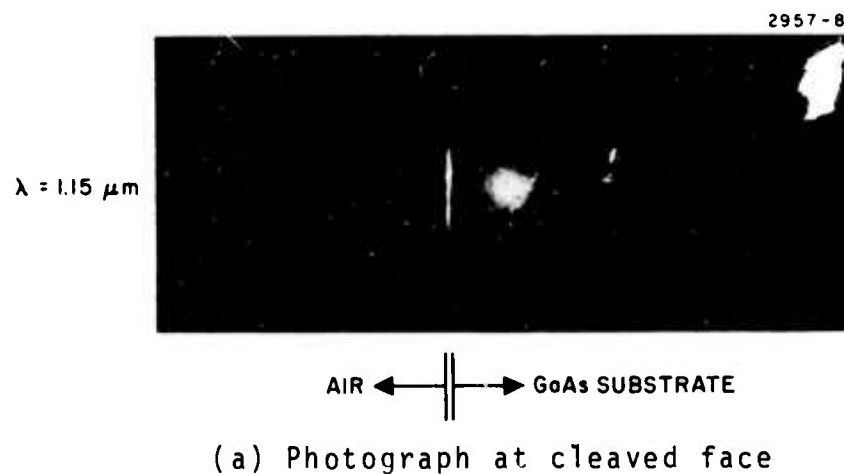


Fig. 4. Waveguided light in a (GaAl)As layer with graded aluminum concentration.

2957-7

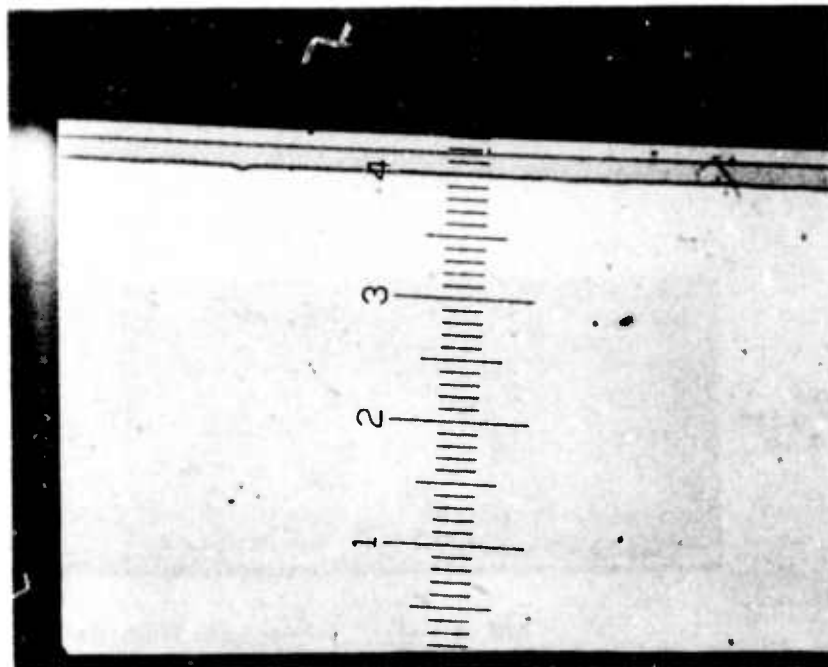


Fig. 5. A double layer of  $\text{Ga}_{1-y}\text{Al}_y\text{As}/\text{Ga}_{1-x}\text{Al}_x\text{As}$  grown on GaAs. Scale is  $2\ \mu/\text{div}$ . LEPI No. 127.

layers with well defined aluminum concentration that can be reproducibly obtained, and (2) The use of the pyrolytic graphite assembly makes the wiping operation at the end of each growth smooth, resulting in scratch-free interface and top surface. Both of these are essential for wave-guiding applications.

### III. INFINITE MELT LIQUID EPITAXY

#### A. Materials Growth

Using the infinite melt technique, a series of layers of  $(\text{Ga}_{1-x}\text{Al}_x)\text{As}$  were grown with increasing aluminum concentration from a melt maintained in our equipment for a period of over two months. The layers grown varied in aluminum concentration from 4% to 40% in  $x$ , the region of interest to integrated optics. The characteristics of the layers were studied in detail; the results demonstrate the versatility and capability of the growth system that we have perfected. The layers obtained by the method are presently being analyzed by the electron microprobe and by optical absorption to compare them with similar ones from the slide bar method.

In our last progress report we have given a detailed description of the use of the infinite melt epitaxial system and the growth  $(\text{GaAl})\text{As}$  using  $\text{Al}_2\text{O}_3$  crucibles. The films obtained had a carrier concentration of  $2 \times 10^{16}/\text{cm}^2$  or higher. The layers had a slight orange-peel appearance, especially when viewed under proper lighting. Since the carrier concentration was higher than what we normally obtain for  $\text{GaAs}$  using quartz crucibles ( $\sim 10^{14}/\text{cm}^3$ ) we decided to improve the growth system to eliminate all possible air leaks. We also proceeded to clean the aluminum oxide crucible more carefully, including a gallium soak to clean the aluminum oxide.

The new growth system has proved to be very satisfactory. It has a larger diameter growth chamber that can house an aluminum oxide crucible within a quartz crucible. The drive for rotating the seed has been refined to permit very slow speeds of less than a rotation per minute and the temperature programmer is capable of cooling the melt at the rate of  $0.1^\circ/\text{min}$ . Starting with a melt of approximately 250 g of Ga saturated as  $\text{GaAs}$ , a series of runs was performed to grow  $(\text{GaAl})\text{As}$  of increasing aluminum concentration.

## B. Epitaxial Layer Characterization

The results of the infinite melt growth series are shown in Table II. After a few initial runs to remove the effects of the newly cleaned tube, the layers stabilized in their characteristics to give a carrier concentration below the  $10^{14}/\text{cm}^3$  with good mobility and very smooth surfaces. Tin was added to bring the level of doping to  $10^{15}/\text{cm}^3$ , and it was gratifying to find the measured doping level to match what would be expected from the segregation coefficient of tin in GaAs solution. After the addition of tin, a series of growth runs were made with addition of aluminum every few days to increase the aluminum concentration. The  $\text{Ga}_{1-x}\text{Al}_x\text{As}$  grown covered the aluminum concentration range of  $x = 0.04$  to  $x = 0.4$ , which is of special interest for integrated optics.

Several facts can be seen easily from the data in the table. The carrier concentration stayed very uniform and reproducible over a period of about 1 month, while aluminum concentration was being progressively increased. The quality of the layers, as given by the Hall measurements, is consistent with what should be expected. The layer quality as evidenced by surface examination and study of the cleaved edges is uniform, smooth, and defect-free. The absorption edge measured for the (GaAl)As agrees with that calculated from the aluminum concentration obtained by the electron microprobe. These results are very significant and prove the capability of the infinite melt technique to produce layers that have the quality necessary for large area substrates for integrated optics applications.

One other noteworthy improvement was achieved using the improved seed rotation capability built into the new system. It had been observed, when the GaAs layers were grown with the seed stationary, that the surface has submicron contour lines at the surface. These appear to be growth features caused by a steady-state pattern in the melt that results in a growth variation at various points on the substrate surface. In the case of (GaAl)As, this is further aggravated by a slight orange-peel effect. We introduced the rotation of the seed as

TABLE II  
(Ga<sub>1-x</sub>Al<sub>x</sub>As) Epitaxial Layer: Characteristics

Layer No.	Aluminum Concentration, X	Layer Thickness, $\mu\text{m}$	Type	Carrier Concentration, $\text{cm}^{-3}$	Mobility, $\text{cm}^2/\text{Vs}$
19	0.04	47	p	$5.5 \times 10^{13}$	310
20	0.04	56	p	$9.0 \times 10^{13}$	319
28	0.07	38	n (Sn)	$2.0 \times 10^{15}$	4338
32	0.07	56	n (Sn)	$2.5 \times 10^{15}$	4652
41	0.13	51	n (Sn)	$2.0 \times 10^{15}$	2979
47	0.40	13	n (Sn)	$8.0 \times 10^{14}$	1724
49	0.40	21	n (Sn)	$3.5 \times 10^{15}$	1840

T1194



a way to eliminate static conditions in the melt and also to avoid any possible depletion of aluminum at the growth front due to the high segregation coefficient of aluminum. The layers obtained with the seed rotation have smooth surfaces with no contour lines. A study of the cleaved cross section indicates that the variation of thickness in a 1-in. long substrate is also reduced below the 10% that normally is observed on a nonrotated substrate.

With the improvements described in the previous paragraphs, the infinite melt system is capable of producing excellent (GaAl)As layers of over  $6 \text{ cm}^2$  with good control of thickness carrier concentration and surface finish. The next step is to design a multicrucible system that can grow several layers in succession. A larger growth system is being assembled that can easily handle two melts. Such a system is indispensable for multilayer growth since no simple technique presently is available to prepare a (GaAl)As layer for epitaxial growth after it is exposed to air. We have, however, demonstrated the possibility of pulling the seed out of the melt and dipping it back in to grow several layers without exposing the (GaAl)As surface to air.

Some electron microprobe measurements have been made on the (GaAl)As layers grown by the infinite melt method. The results are shown in Figs. 6 and 7.

It can be seen from Fig. 6 that the surface variation of aluminum concentration is  $\approx 5$  to  $6\%$  for samples 41 and 61. Neglecting one or two extreme points in each case, the variation is even less  $\approx \pm 2$  to  $3\%$ . This is well within the errors of measurement using the microprobe for the type of surface involved. When the slide bar epitaxial layer is thin enough and the central areas of the layer are examined we see that these layers are almost as good as the infinite melt layers. However, the variations are more random and the electrical properties in Tables I and II show the difference in quality even in these cases.

Figure 6 shows the variation of aluminum concentration on a bevel without the corrections mentioned in the previous section for the junction region. The bevel in this case is a  $3^\circ$  one, however, and this reduces the error, and the profile is more amenable to measurement.

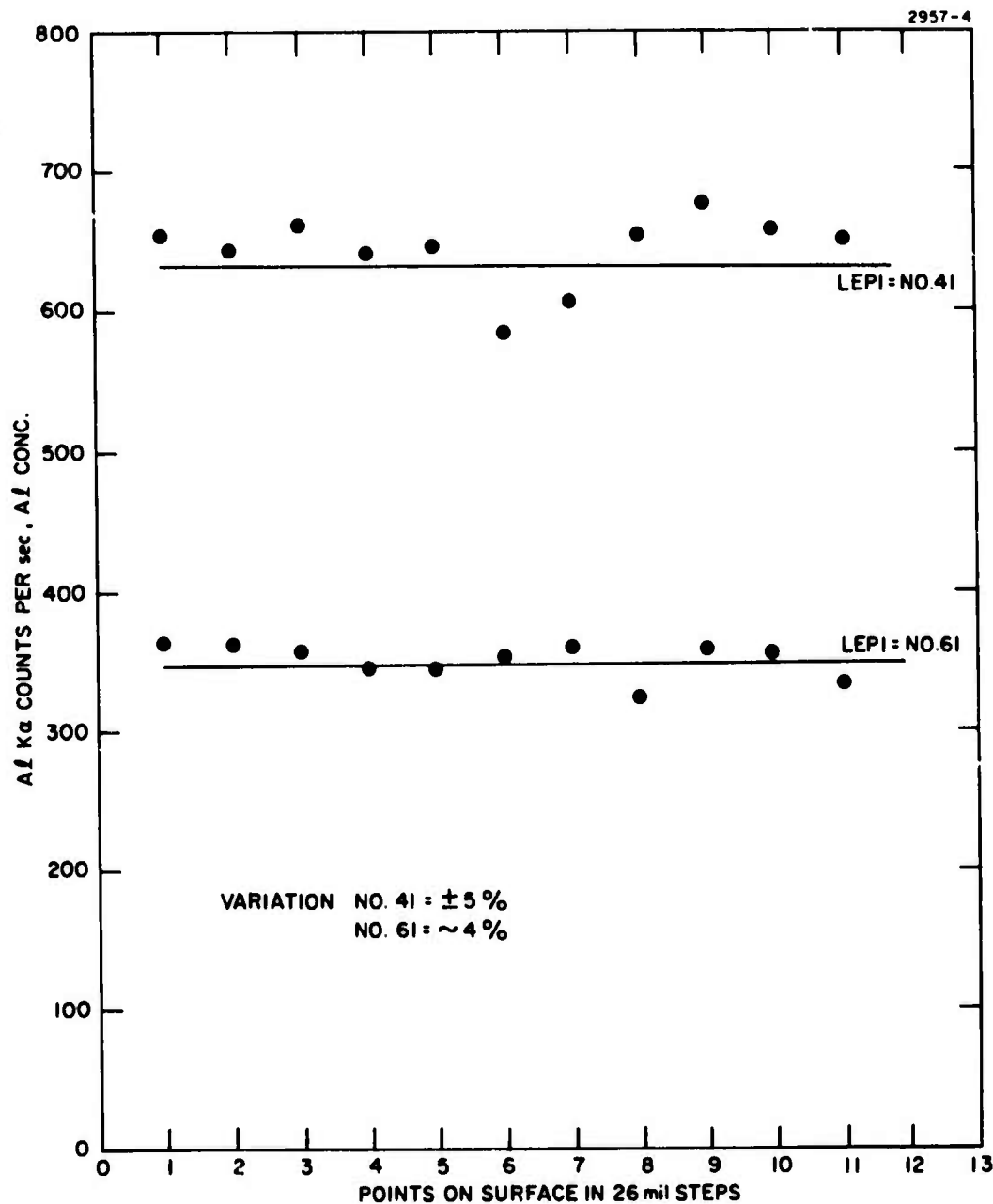


Fig. 6. Aluminum concentration profile on  $\omega$  melt LEPI layers (surface of epilayer).

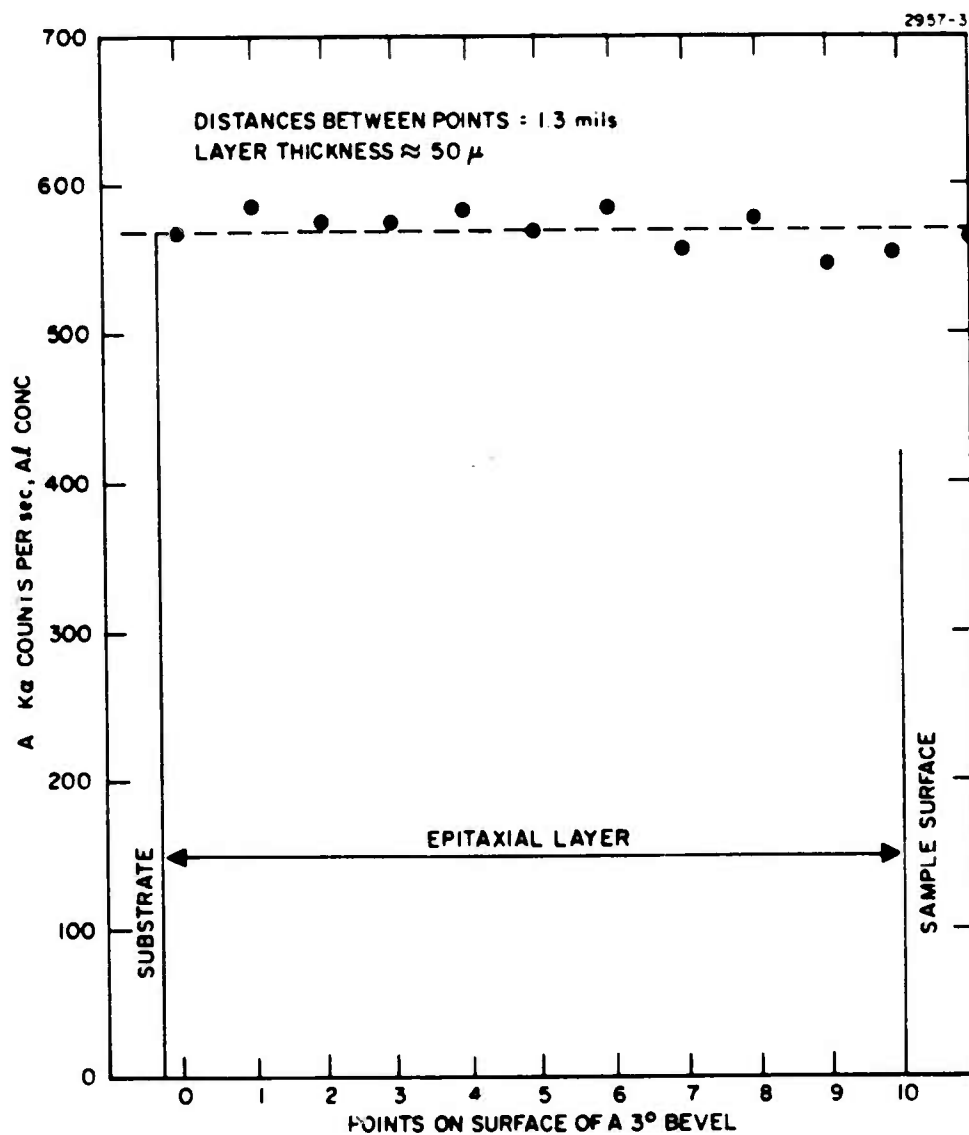


Fig. 7. Aluminum concentration profile in  $\infty$  melt liquid epitaxial layers on a 3° bevel in cross section (LEPI No. 41).

It is interesting to note that within the limits of the technique the infinite melt technique can produce 50  $\mu\text{m}$  thick layers with an almost invariant aluminum concentration in the cross section of the layer. If we compare the measurements in this report with those in our previous ones, the present samples are seen to have a smoother profile. This comes primarily from using a layer melt and also including rotation of the substrate at a controlled rate during growth. The results support our thesis that good substrate layers of (GaAl)As, with compositional uniformity and homogeneity and with smooth surfaces, can be produced by the infinite melt technique. These substrates can be used for monolithic technology in integrated optics, a necessary step if the full benefits of the new field are to be realized. The quality of the layers is further emphasized by the excellent bulk properties shown in Table II for impurity concentrations and carrier mobilities.

During the next quarter we intend to grow more layers of (GaAl)As by the two methods and compare them with greater precision by improving the beveling technique and working with a series of electron beam energies to get a more accurate determination of the aluminum concentration. These samples will also be evaluated by optical measurements.

#### IV. DEVICE ELEMENTS

##### A. Analysis of Proton Implanted Integrated Waveguide/Detector

In Semiannual Technical Report No. 2 we discussed a number of device elements for optical integrated circuits. One of these that is of particular interest to us is the integrated waveguide/detector. A fundamental problem in the fabrication of this device is that of wavelength incompatibility. An integral detector formed in a waveguide which transmits light of a certain wavelength with low loss will generally have an extremely low quantum efficiency because the bandgap will be, of necessity, too large to allow substantial interband absorption. Under a company funded program we have used proton bombardment to locally shift the absorption edge of GaAs to a longer wavelength in the active volume of the detector. Thus, we have been able to fabricate integrated waveguide/detectors in GaAs. This work has recently been published<sup>1</sup> and a reprint of the paper is included as Appendix (A) of this report. Since this technique appear useful in the case of (GaAl)As waveguides as well, we have evaluated the projected performance of a proton implanted detector during the last quarter of this contract period. Experimental data compiled in the company-funded research program (Appendix A) were used in the evaluation.

Figure 8 depicts the device geometry. The optical waveguiding structure consisted of a  $3.5 \mu$  thick n-type (S-doped,  $n = 2.8 \times 10^{16} \text{ cm}^{-3}$ ) epitaxial film grown on a degenerate n-type substrate ( $n = 1.25 \times 10^{18} \text{ cm}^{-3}$ ). Good optical confinement for the guide thickness used resulted from the guide-substrate refractive index discontinuity generated by the plasma depression effect; prior to implantation, optical attenuation at  $1.15 \mu$  was measured to be  $1.3 \text{ cm}^{-1}$  and could be accounted for by consideration of free carrier substrate penetration losses. The aluminum Schottky barrier was 11 mils square.

The principle of operation of the detector is similar to that of conventional p-n or p-i-n junction photodetectors: Upon the application of a reverse bias to the Schottky barrier, a depletion layer is produced which, given sufficient reverse bias, extends across that high resistivity

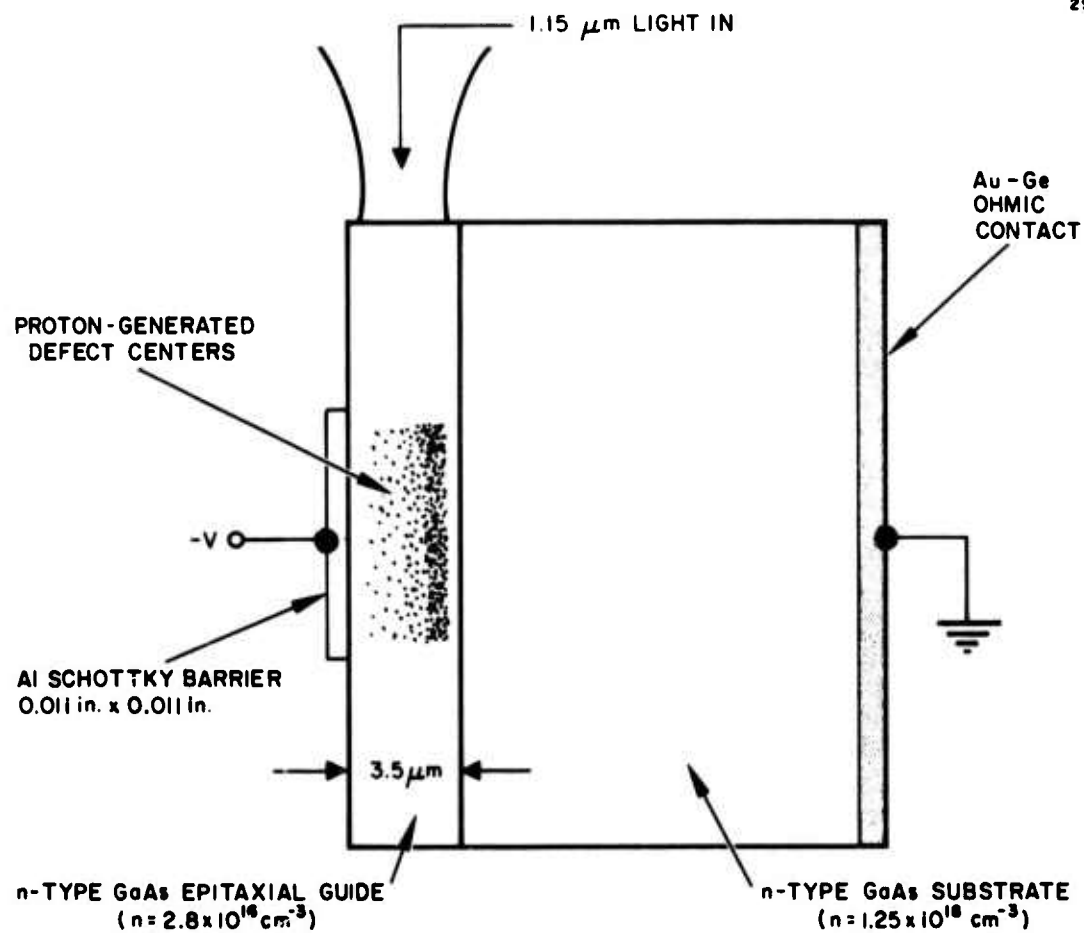


Fig. 8. Proton-implanted integrated optical detector — device geometry.

waveguiding layer to the lower resistivity substrate. Any dipole transitions made possible by radiation-produced defect levels then generate free carriers which are swept out of the depletion layer, thereby causing current to flow through an external circuit. The situation is depicted schematically in Fig. 9. By insuring that the radiation-induced damage extends over most of the waveguiding layer and by choosing epitaxial material of high purity (in order to allow the widest possible depletion region), maximum detector efficiency can be obtained over a given interaction length.

When illuminated, as shown in Fig. 8, by a Spectra Physics model 120 He-Ne laser emitting 0.75 MW of optical power at 1.15  $\mu\text{m}$ , a particular (typical) detector generated a current of approximately  $1.5 \times 10^{-5}$  A when biased to near reverse breakdown voltage. Hence, the number of electrons swept out of the depletion layer per second was

$$e = \frac{1.5 \times 10^{-5}}{1.602 \times 10^{-19}} = 0.935 \times 10^{14} \text{ electrons/s}$$

In this integral waveguide/detector the waveguide was implanted with 300 keV protons, the total integrated flux of which was  $2 \times 10^{15} \text{ cm}^{-2}$ . The sample was then annealed at 500°C for 30 min. in order to allow some optical transmission through the damaged waveguide; residual, defect-associated losses were measured to be  $\approx 15 \text{ cm}^{-1}$  based on a comparison of the optical attenuation before and after implantation and annealing. The Schottky barrier was 8 mils from the waveguide input face. Thus, taking the output power of the laser to be 0.75 MW and the overall waveguide insertion loss to be 50% (including both reflection at the input face, 30%, and waveguide mode coupling loss, 20%) and assuming that the entire guided beam passed under the Schottky barrier in question, the number of photons per second that were lost while traversing the detector is given by:

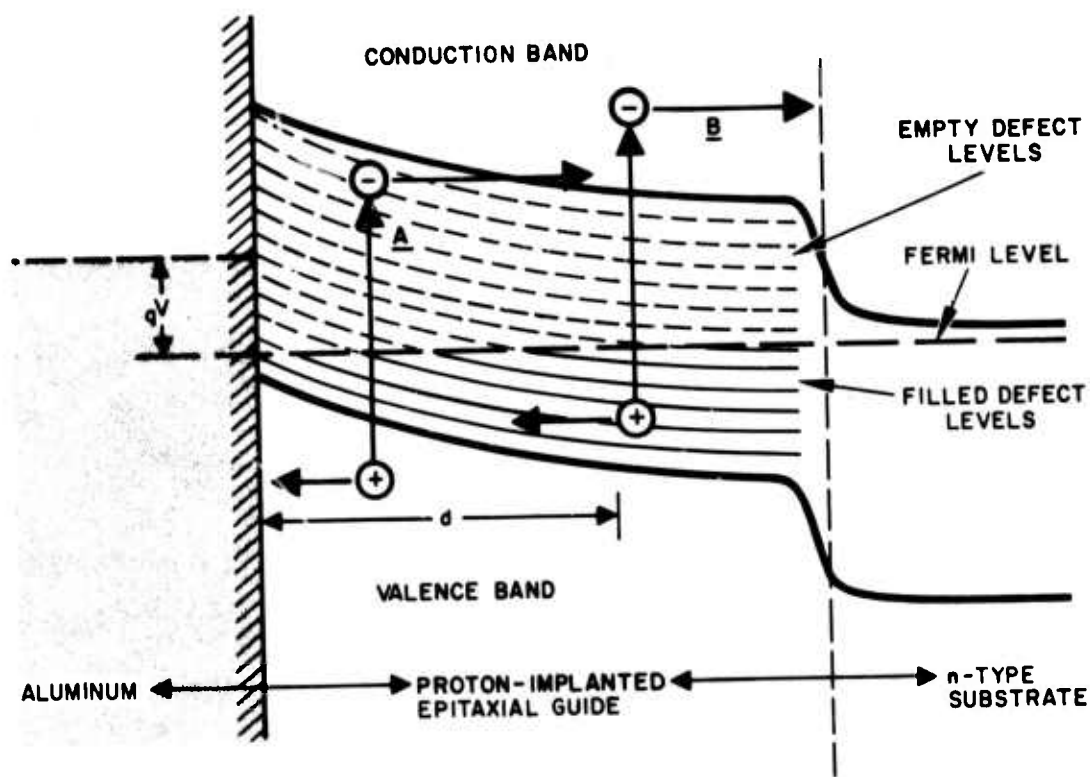


Fig. 9. Principle of operation of integrated optical detector: Upon the application of a reverse bias ( $V$ ) electrons liberated by transitions labeled "A" and "B" are swept out of depletion layer  $d$  resulting in the flow of current.



$$P = \frac{(0.75 \times 10^{-3})(0.5) \exp(-15 \times 0.0025 \times 8)[1 - \exp(-15 \times 0.0025 \times 11)]}{(1.08)(1.602 \times 10^{-19})}$$

$$= 5.42 \times 10^{14} \text{ photons/s}$$

The internal quantum efficiency of the detector was, therefore,

$$\left(\frac{e}{p}\right) \times 100 = 17\%$$

Two factors probably contributed to this relatively low quantum efficiency, namely dissipative absorption and incomplete layer depletion. Calorimetric absorption measurements made by Stein<sup>2</sup> indicate that essentially all of the optical attenuation observed in proton implanted GaAs can be attributed to absorption rather than diffuse scattering. However, Stein's measurements cannot distinguish between absorption which generates a carrier and absorption resulting from dissipative centers such as the microscopic metallic inclusions reported by McNichols in neutron bombarded GaAs.<sup>3</sup> Calculations made by Stein<sup>2</sup> indicate that possibly as much as 60% of the total bombardment induced absorption at 1.15  $\mu\text{m}$  wavelength could be attributed to dissipative absorption and scattering, with only the remaining 40% resulting in the promotion of trapped electrons to the conduction band. This effect would impose a fundamental limit to the quantum efficiency of a proton implanted detector, but the 60% value calculated by Stein is a "worst case" estimate and, in any case, the effect diminishes at wavelengths closer to the bandedge wavelength. For example, based on Stein's calculation the dissipative absorption would be at most 45% of the total at 1.0  $\mu\text{m}$ .

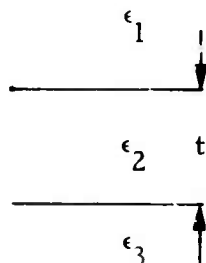
A second factor action to reduce quantum efficiency is incomplete layer depletion. The residual free carrier concentration in the implanted waveguide being presently considered, as determined by the capacitance-voltage technique, was found to be  $\approx 2.8 \times 10^{16} \text{ cm}^{-3}$ , or approximately the original preimplantation value. As a result, the width of the depletion layer (for a reverse bias of 30 V) was only 2.9  $\mu\text{m}$ ,

compared to the waveguide thickness of  $3.5 \mu\text{m}$ . Calculations based on optical mode shape indicate that, under these circumstances, only approximately 90% of the electrons liberated from trapping levels are exposed to the influence of the electric field generated within the depletion region. This effect can, of course, be minimized by using a thinner or more lightly doped waveguide, or altered proton dose/energy combination to achieve full depletion.

The fabrication of a proton implanted detector integrally within a (GaAl)As waveguide can be accomplished by using the same techniques that have been applied successfully to GaAs. Probably the most useful integral waveguide/detector combination would be one that could function satisfactorily at a wavelength of  $0.9 \mu\text{m}$ , and, hence, could be used with a GaAs LED or laser source. As discussed in Semiannual Report No. 2 (summary appears in Table II of that report) this requires minimum aluminum concentrations of 7% in the waveguide and 10% in the substrate, for single-mode propagation in a guide of thickness  $t = 2.5 \mu\text{m}$  with attenuation  $= 2 \text{ cm}^{-1}$ . The region in which the detector volume is desired would be implanted with 250 keV protons in a dose  $10^{16}/\text{cm}^2$  to produce the required absorptive centers. The exact distribution of the defect-associated energy states within the bandgap of the (GaAl)As is not known. However, assuming their spacing from the bandedge scales linearly with bandgap one estimates an absorption coefficient in the proton implanted region of  $\alpha = 5 \times 10^3 \text{ cm}^{-1}$  at  $0.9 \mu\text{m}$ , based on the data measured by Stein<sup>2</sup> for GaAs. This implies that the length of the detector in the direction of propagation should be at least  $15 \mu\text{m}$  to obtain essentially total absorption. Again, based on extrapolation of Stein's GaAs data one would project that possibly as much as 40% of the total absorption would go into dissipative processes rather than carrier generation. However, it should be emphasized that this percentage represents an estimated upper limit rather than a predicted value. Thus, if the carrier concentration in the waveguide is kept low enough ( $\leq 10^{16} \text{ electrons/cm}^3$ ) that the detector volume can be completely depleted by the reverse biased Schottky diode, all of the carriers generated will be swept out, giving an estimated internal quantum efficiency of at least 60%.

## B. Analysis of "Leaky" Waveguides

To date we have considered only confined propagation waveguides in which the dielectric constants obey



$\epsilon_1 < \epsilon_2 > \epsilon_3$ . In some cases it may be easier to fabricate a guide where  $\epsilon_1 < \epsilon_2 < \epsilon_3$ . This would be the case, for example, if layer 3 is a GaAs substrate while 2 is  $\text{Ga}_{1-x}\text{Al}_x\text{As}$  (1 is air). Such a structure is inherently lossy, since no total internal reflection can take place at the 2-3 interface. We will show below that for moderate values of  $t$  the "leak" loss can be reduced to a tolerable level.

Consider the problem of propagation in the dielectric configuration of Fig. 10

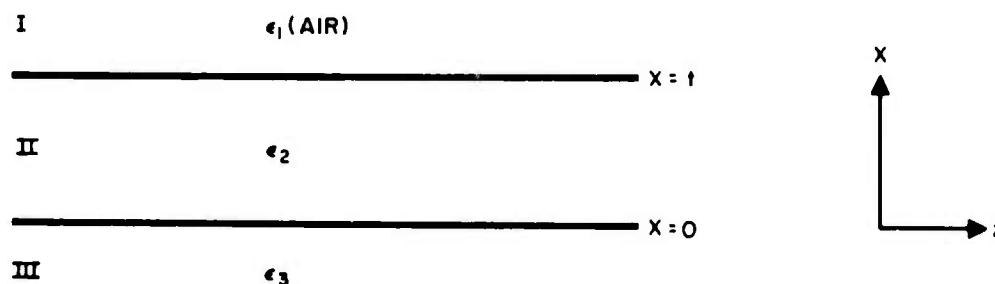


Fig. 10. Dielectric waveguide configuration.

where

$$\epsilon_3 > \epsilon_2 > \epsilon_1, \quad \epsilon_i = \epsilon_0 n_i^2$$

If we assume solutions of the form

$$\text{Region I} \quad E_y = A \exp[i(h_1 x + \gamma z - \omega t)] \quad x \geq t$$

$$\text{Region II} \quad E_y = \left\{ B \cos(h_2 x) + c \sin(h_2 x) \right\} \exp[i(\gamma z - \omega t)] \quad 0 \leq x \leq t$$

$$\text{Region III} \quad E_y = D \exp[i(-h_3 x + \gamma z - \omega t)] \quad x \leq 0$$

Then it follows from the wave equation

$$\left( \gamma^2 + \frac{\partial^2}{\partial x^2} \right) E_y + k_i^2 E_y = 0 \quad (1)$$

$$k_i^2 = \omega^2 \mu \epsilon_i = k^2 n_i^2 \quad (k = \frac{2\pi}{\lambda})$$

Applying eq. (2) to regions I, II, and III gives

$$h_1^2 = k_2^2 \left( \frac{\epsilon_1}{\epsilon_2} \right) - \gamma^2$$

$$h_2^2 = k_2^2 - \gamma^2 \quad (2)$$

$$h_3^2 = \frac{\epsilon_3}{\epsilon_2} k_2^2 - \gamma^2$$

Matching  $E_y$  and  $\frac{\partial E_y}{\partial x}$  at  $x = 0$  and  $x = t$  gives

$$A \exp(h_1 t) - B \cos(h_2 t) - C \sin(h_2 t) = 0$$

$$h_1 A \exp(h_1 t) - i B h_2 \sin(h_2 t) + i C h_2 \cos(h_2 t) = 0 \quad (3)$$

$$B - D = 0$$

$$i h_2 C - h_3 D = 0$$

Setting the determinant of coefficients of A, B, C, and D in eq. (3) equal to zero given

$$\tan(h_2 t) = -i(h_1 h_2 + h_3 h_2) / (-i h_2^2 + h_1 h_3) \quad (4)$$

To obtain an approximate solution we will assume that the waveguide is "large" so that  $k_2 a \rightarrow \infty$  it follows from the second of eq. (2) that in the same limit  $\gamma \rightarrow k_2$

and

$$h_1 \approx i k_2 \left( 1 - \frac{\epsilon_1}{\epsilon_2} \right)^{1/2} \quad (5)$$

$$h_3 \approx k_2 \left( \frac{\epsilon_3}{\epsilon_2} - 1 \right)^{1/2}$$

so that

$$k_2, h_3, h_1 \gg h_2$$

We can thus approximate eq. (4) by

$$h_2 t = \tan^{-1} \left[ i \left( \frac{h_2}{-h_1} - \frac{h_2}{h_3} \right) \right] + n\pi \quad n = 0, 1, 2,$$

(In view of eq. (7), the  $n = 0$  solution is discarded since  $A \sin(h_1 x) + B \cos(h_1 x) = \text{constant}$  and we only use the solution  $n = 1, 2, 3, \dots$ )

$$\begin{aligned} & \approx \tan^{-1} \left\{ i \left( \frac{-h_2}{ik_2 \left( 1 - \frac{\epsilon_1}{\epsilon_2} \right)^{1/2}} - \frac{h_2}{k_2 \left( \frac{\epsilon_3}{\epsilon_2} - 1 \right)^{1/2}} \right) \right\} + n\pi \\ & = \tan^{-1} \left\{ -\frac{h_2}{k_2} E_2 - i \frac{h_2}{k_2} E_3 \right\} + n\pi \end{aligned} \quad (6)$$

$$E_2 = \left( \frac{1}{1 - \frac{\epsilon_1}{\epsilon_2}} \right)^{1/2}, \quad E_3 = \left( \frac{1}{\frac{\epsilon_3}{\epsilon_2} - 1} \right)^{1/2}$$

Since  $E_2$  and  $E_3$  are 0 (1) and  $k_2 \gg h_2$ , eq. (6) can be written as

$$h_2 t \approx -h_2 t \frac{E_2}{k_2 t} - i h_2 t \frac{E_3}{k_2 t} + n\pi$$

$$h_2 t \left( 1 + \frac{E_2}{k_2 t} + i \frac{E_3}{k_2 t} \right) = n\pi \quad n = 1, 2, 3, \dots$$

$$h_2 t \approx n\pi \left[ 1 - \frac{E_2}{k_2 t} - i \frac{E_3}{k_2 t} \right] \quad (7)$$

Substituting eq. (7) into the second of Eq. (2) given

$$y_{TE} = k_2 \left[ 1 - \frac{n^2 \pi^2}{2k_2^2 t^2} \left( 1 - \frac{2E_2}{k_2 t} \right) \right] + i \frac{n^2 \pi^2 \times^2 E_3}{2k_2 t^2 k_2 t}$$

The exponential intensity decay coefficient is thus

$$\alpha_{TE} = 2 \operatorname{Im} y_{TE} = \frac{2k_2 n^2 \pi^2 E_3}{(k_2 t)^3}, \quad n = 1, 2, 3, \dots$$

$$k_2 = \frac{2\pi}{\lambda} n_2, \quad E_3 = \frac{1}{\sqrt{\frac{\epsilon_3}{\epsilon_2} - 1}} = \frac{1}{\sqrt{\frac{n_3^2}{n_2^2} - 1}}$$

$\lambda$  = vacuum wavelength

for

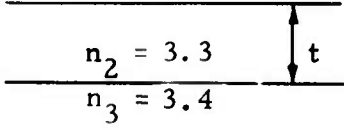
$$\Delta n = n_3 - n_2 \ll n_2, n_3$$

$$\alpha_{TE} \approx \frac{1}{2\lambda \left(\frac{t}{\lambda}\right)^3 n^2 \sqrt{\frac{2\Delta n}{n}}}$$

Calculated values for  $\alpha$  in the particular case where  $n_2 = 3.3$  and  $n_3 = 3.4$  are shown in Table III.

TABLE III

Calculated Values of  $\alpha$  for  $\lambda = 0.8 \mu$ ,  $n_2 = 3.3$ 

$n = 1$  $\alpha \approx \frac{1}{2\lambda \left(\frac{t}{\lambda}\right)^3 n^2 \sqrt{\frac{2\Delta n}{n}}}$		
$t/\lambda$	$t(\mu m)$	$\alpha(cm^{-1})$
1	0.8	2331
2	1.6	291
3	2.4	86
4	3.2	36
5	4	18
6	4.8	10.8
7	5.6	6.8
8	6.4	4.6
9	7.2	3.2
10	8	2.33
13	10.4	1.06

The data of table III show that useful integrated optics devices can be fabricated using leaky waveguides provided the guide height is  $t \lesssim 10 \mu$ . The losses due to leaks become  $< 1 cm^{-1}$  for typical aluminum concentration  $> 20\%$ .



## V. FUTURE PLANS

In the coming half year, we expect to continue the growth and characterization of epitaxial layers produced by both the limited-melt and infinite-melt techniques. Detailed electron beam microprobe measurements will be made of the aluminum concentration profile versus depth in the epitaxial layers. Greater precision will be obtained in these measurements by improving the beveling technique and working with a series of electron beam energies. Particular attention will be directed toward layers capable of waveguiding light. Waveguides of both the graded aluminum concentration and multilayer types will be evaluated. Optical attenuation and mode shape also will be measured and correlated with the aluminum concentration profile data.

The device elements task will continue to be directed toward exploring the relationships between device requirements and material properties. We intend to experimentally test the theoretical calculations of leaky waveguide projected performance which were presented in this report. This will be done by measuring optical attenuation and mode shape in thick ( $>10\text{ }\mu\text{m}$ ) (GaAl)As layers grown on GaAs substrates.

## REFERENCES

1. H. Stoll, A. Yariv, R. G. Hunsperger and G. L. Tangonan, Appl. Phys. Lett. 23, 664 (1973).
2. H. J. Stein, Proceedings of the International Conference on Ion Implantation in Semiconductors and Other Materials, Dec 11-14 1972, Yorktown Heights, New York (Plenum Press, N.Y., 1973).
3. J. L. McNichols and W. S. Ginell, J. Appl. Phys., 38, 656 (1967).

## APPENDIX

### Proton-implanted optical waveguide detectors in GaAs

H. Stoll and A. Yariv

California Institute of Technology, Pasadena, California 91109

R. G. Hunsperger and G. L. Tangonan

Hughes Research Laboratories, Malibu, California 90265

(Received 17 August 1973)

Defect levels introduced by implanting GaAs with high energy protons give rise to optical absorption at wavelengths greater than that of the normal absorption edge at  $0.9 \mu$ . Optical waveguide detectors may be fabricated by taking advantage of this absorption mechanism in the presence of a Schottky barrier depletion layer. Detector response times less than 200 ns and external quantum efficiencies of 16% have been observed.

In a continuing program to build circuit components for integrated optics we have investigated the possibility of fabricating optical detectors by proton implantation of GaAs dielectric waveguides. The basic principle is as follows: A small volume of an epitaxial GaAs waveguide, such as the one shown in Fig. 1, is implanted with protons. Structural disorder created by the implantation process causes the previously low-loss waveguide to become highly lossy for radiation around  $1 \mu$ . One of the mechanisms responsible for this absorption is the liberation of free carriers which had become trapped at defect centers. A photodetector results when these carriers are swept through the depletion layer generated by a reverse-biased Schottky barrier which has been deposited over the implanted region as shown in Fig. 1. We report below the fabrication of integrated optical detectors based on this principle. The detectors have been found to be sensitive to light of wavelengths  $> 0.9 \mu$ , a wavelength which can be transmitted nearly unattenuated by the GaAs guides used. The optical waveguide structure consisted of a  $3.5\text{-}\mu\text{m}$ -thick  $n$ -type (S-doped,  $n \approx 10^{18}/\text{cm}^3$ ) epitaxial film grown on a degenerate  $n$ -type substrate ( $n > 1.25 \times 10^{18}/\text{cm}^3$ ). The guide-substrate refractive index discontinuity generated by the plasma depression effect allowed good optical confinement for the particular guide thickness used; prior to proton implantation optical attenuation at  $1.1 \mu$  was measured to be  $1.3 \text{ cm}^{-1}$  and could be accounted for by consideration of free carrier substrate penetration losses.

As shown in Fig. 1, a small volume of the waveguide

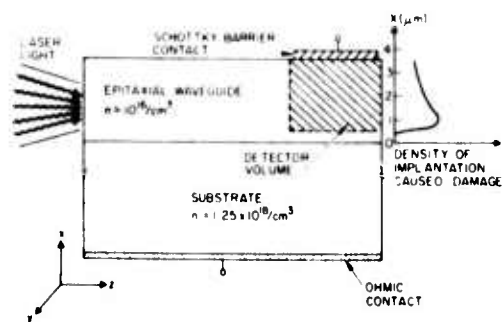


FIG. 1. Diagram of proton-implanted optical waveguide detector.

structure was proton bombarded to form the waveguide detector; 300-keV protons were used, the total integrated flux of which was  $2 \times 10^{15}/\text{cm}^2$ . The damage layer which resulted was approximately  $3 \mu$  thick with a damage peak occurring about  $2.5 \mu$  below the surface.

The implanted waveguide was then annealed at  $500^\circ\text{C}$  for 30 min in order to allow some optical transmission through the damaged region; residual losses in this region were measured to be  $\approx 15 \text{ cm}^{-1}$  based on a comparison of the optical attenuation before and after implantation and annealing. Finally, 11-mil-square Al Schottky barriers were evaporated in a waffle pattern over the implanted area.

The principle of the operation of this device is similar to that of conventional  $p\text{-}n$  or  $p\text{-}i\text{-}n$  junction photodetectors.

Upon the application of a reverse bias to the Schottky barrier, a depletion layer is produced which, given sufficient reverse bias, extends across the high-resistivity waveguiding layer to the lower-resistivity substrate. Any dipole transitions made possible by radiation

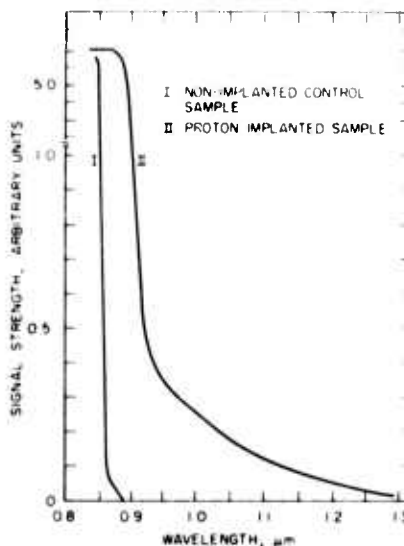


FIG. 2. Photoreponse of optical waveguide detector as a function of wavelength.

Preceding page blank

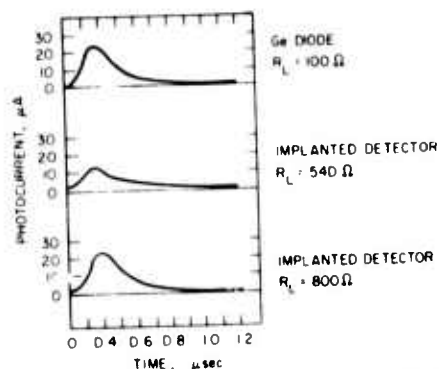


FIG. 3. Response of waveguide detector to pulsed optical signal.

tion-produced defect levels generate free carriers which are swept out of the depletion layer, thereby causing current to flow through an external circuit. By ensuring that the radiation-induced damage extends over most of the waveguiding layer and choosing epitaxial material of high purity, maximum efficiency can be obtained over a given interaction length.

Measurements of the photosensitivity of both unimplanted and implanted annealed samples are shown in Fig. 2. Transparent Au barriers, sputter deposited on the surface, were used to measure sensitivity as a function of wavelength. A monochromator-filtered incandescent light source was focused through the transparent Au layer into the active volume of the detectors. The curve for the irradiated sample reveals a defect-associated energy level distribution within the band gap, as well as a shift of the effective absorption edge to lower energies. Calorimetric measurements<sup>2</sup> made on proton-irradiated GaAs at 1.06  $\mu\text{m}$  indicate that substantially all of the implantation-induced optical attenuation in the 1- $\mu\text{m}$ -wavelength region can be attributed to absorption as opposed to diffuse scattering. The origin of this absorption is thought to be disorder-induced band tailing. The possibility that it is due, at least in part, to the excitation of electrons from energy levels associated with As (or Ga) vacancy complexes is strong, particularly in view of the fact that free carrier compensation by proton implantation appears to be Fermi-level dependent.<sup>3,4</sup>

An attempt was made to measure detector rise and fall times at 1.06  $\mu\text{m}$  using an acoustically Q-switched Nd:YAG laser focused into a cleaved face of the waveguide structure of Fig. 1. The pulse response of the implanted detector is compared to that of a commercial Ge (Philco L4521) detector in Fig. 3. In both cases the

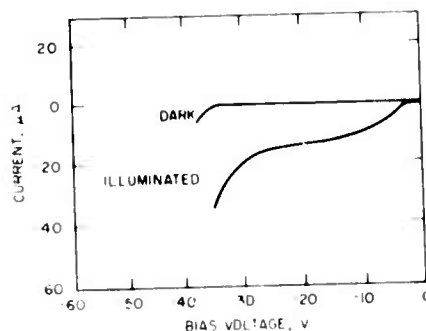


FIG. 4. Reverse bias current-voltage characteristics of waveguide detector.

rise and fall times appeared to be  $\sim 200$  and  $\sim 400$  ns, respectively. Reducing the size of the load resistors used merely decreased the signal strength; the pulse shapes remained the same. Since the Ge detector response is in the GHz range, it was concluded that the rise and fall times measured were a function of the Q-switched laser and did not represent limits of the implanted detector.

Figure 4 shows  $I$ - $V$  curves for a reverse-biased implanted detector under dark and 1.15- $\mu\text{m}$  illumination conditions. The measured external quantum efficiency at 1.15  $\mu\text{m}$ , 294°K, and a reverse bias of 20 V was about 16%. This number should increase as optimal proton damage profile and heat treatment conditions are approached for a given waveguiding configuration.

In conclusion we have demonstrated a simple technique for fabricating integrated optical detectors sensitive at wavelengths  $> 0.9 \mu\text{m}$  using proton implantation. Device performance is promising and should improve as implantation and heat treatment procedures are refined.

The authors would like to thank Dr. W. C. Holton of Texas Instruments for providing the epitaxial GaAs material.

<sup>1</sup>D. Hall, A. Yariv, and E. Garmire, *Appl. Phys. Lett.* 17, 127 (1970).

<sup>2</sup>H. J. Stein, *Proceedings of the International Conference on Ion Implantation in Semiconductors and Other Materials*, Yorktown Heights, 1972 (Plenum, New York, 1973).

<sup>3</sup>H. Stoll, E. Garmire, A. Yariv, and R. G. Hunsperger (unpublished).

<sup>4</sup>K. Wohlenben and W. Beck, *Z. Naturforsch.* 219, 1057 (1966).